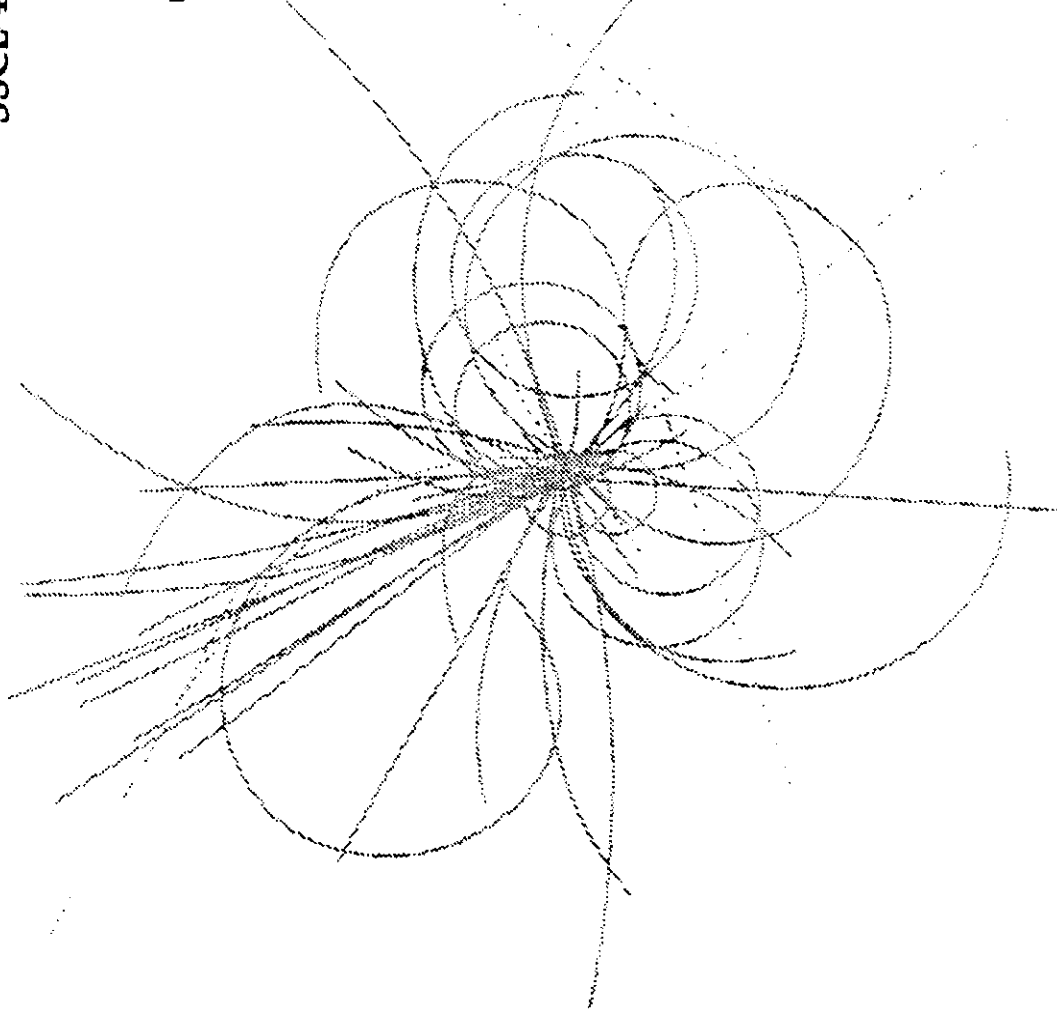


conf 91/188

SSCL-487

SSCL-487

Superconducting Super Collider Laboratory



Status of 4-cm-Aperture, 17-m-Long SSC Dipole R&D Program at BNL Part II: Mechanical Behavior

A. Devred, et al.

June 1991

**STATUS OF 4-CM-APERTURE, 17-M-LONG SSC DIPOLE MAGNET
R&D PROGRAM AT BNL PART II: MECHANICAL BEHAVIOR***

A. Devred, T. Bush, R. Coombes, J. DiMarco, C. Goodzeit, J. Kuzminski, M. Puglisi,
P. Radusewicz, P. Sanger, R. Schermer, G. Spigo, J. Tompkins, J. Turner, Z. Wolf,
Y. Yu, and H. Zheng

Superconducting Super Collider Laboratory†
2550 Beckleymeade Ave.
Dallas, TX 75237

T. Ogitsu

SSC Laboratory and
KEK National Laboratory for High Energy Physics
1-1 Oho, Tsukuba-shi
Ibaraki-ken, Japan

M. Anarella, J. Cottingham, G. Ganetis, M. Garber, A. Ghosh, A. Greene, R. Gupta,
J. Herrera, S. Kahn, E. Kelly, A. Meade, G. Morgan, J. Muratore, A. Prodell, M. Rehak, E. P. Rohrer,
W. Sampson, R. Shutt, P. Thompson, P. Wanderer, and E. Willen

Brookhaven National Laboratory
Upton, New York 11973

M. Bleadon, R. Hanft, M. Kuchnir, P. Mantsch, P. O. Mazur, D. Orris, T. Peterson, and J. Strait

Fermi National Accelerator Laboratory‡
Batavia, Illinois 60510

J. Royet, R. Scanlan, and C. Taylor

Lawrence Berkeley Laboratory§
Berkeley, California 94720

June 1991

*Presented at the Cryogenics Engineering Conference, University of Alabama, Huntsville, Alabama, June 10-14, 1991.

†Operated by the Universities Research Association, Inc., for the U.S. Department of Energy under Contract No. DE-AC35-89ER40486.

‡This work supported by the U. S. Department of Energy, under Contract No. DE-AC02-76CH03000.

§This work supported by the U. S. Department of Energy, under Contract No. DE-AC03-76SF00098.

ABSTRACT

Over the last year-and-a-half, several 4-cm-aperture, 17-m-long dipole magnet prototypes were built by Brookhaven National Laboratory (BNL) under contract with the Superconducting Super Collider (SSC) Laboratory. These prototypes are the last phase of a half-decade-long R&D program, carried out in collaboration with Fermi National Accelerator Laboratory and Lawrence Berkeley Laboratory, and aimed at demonstrating the feasibility of the SSC main ring dipole magnets. They also prepare the way for the 5-cm-aperture dipole magnet program to be started soon. In this paper, we analyze the mechanical behavior of the BNL prototypes during cool-down and excitation, and we attempt to relate this behavior to the magnet features. The data reveal that the mechanical behavior is sensitive to the vertical collar-yoke interference, and that the magnets exhibited somewhat erratic changes in coil end-loading during cool-down.

INTRODUCTION

This is the second of a series of papers reviewing the 4-cm-aperture, 17-m-long Superconducting Super Collider (SSC) dipole magnet R&D program at Brookhaven National Laboratory (BNL). In the first paper,¹ we reported on the design and assembly of the five most recent prototypes. In this paper, we report on the mechanical behavior during cool-down and excitation of the same five magnets, and we attempt to relate this behavior to the construction features. The quench performance, and how it is affected by the mechanical behavior, will be described elsewhere.²

The five magnets discussed here were produced by BNL. Three of them (DD0026, DD0027, and DD0028) were cold-tested at Fermi National Accelerator Laboratory (FNAL);^{3,4} the other two (DC0201 and DC0204) were cold-tested at BNL. These magnets rely on the BNL *line-to-line fit* design, in which part of the support against the radial component of the Lorenz force is provided by the yoke. The main variants in their features are summarized in Table I. Magnets DD0026 through DD0028 used *round* collars designed to perfectly match the inner boundary of the yoke at room temperature. Magnets DC0201 and DC0204 used *anti-ovalized* collars designed to compensate for excess vertical deflection of the collared coil after assembly. Extra shims were added to the tops and bottoms of DC0204 collars to prevent the loss of vertical contact between the collared coil and the yoke in the cold state. The collar material was Nitronic-40 stainless steel for all magnets except DD0026, which used Kawasaki stainless steel. All magnets were equipped with the standard instrumentation of the SSC dipole magnet prototypes, including voltage taps to locate the quench origins and two types of calibrated strain gauges: 1) beam-type strain-gauge transducers to measure the azimuthal pressure exerted by the coil against the collar poles, and 2) "bullet" gauge assemblies to measure the force exerted by the coil against the end plates.⁵ A detailed presentation of the design concepts and of the various magnet features can be found in Reference 1.

The mechanical data reported here are those measured by the two types of strain gauges throughout cool-down and excitation. The cool-down data are monitored at regular time intervals by a slow data logger system. The excitation data are taken during specific current cycles called *strain-gauge runs*. A strain-gauge run consists of ramping the current step-by-step up to a maximum value, then down to zero, reading out the strain gauges at each step; the step increments are usually equally spaced in current squared. (The first magnet excitation after cool-down to a current of the order of the operating current is always a strain-gauge run). In the three sections of this paper, we shall review the inner-layer stress data, the outer-layer stress data, and the end-force data. Each of the three sections will be divided into two subsections, dealing with the change during cool-down and the change during excitation.

(The change during cool-down results from the differences in thermal shrinkage between the various magnet parts. The change during excitation results from the Lorenz force on the conductors.)

Table I. Variants in Design Features of Most Recent BNL 4-cm Aperture, 17-m-Long Collider Dipole Prototypes

	DD0026	DD0027	DD0028	DC0201	DC0204
Inner Conductor Copper-to-Superconductor Ratio	1.44	1.48	1.52	1.52	1.29
Inner Conductor Critical Current at 4.22K and 7T*	7465 A	7822 A	7893 A	7893 A	8368 A
Epoxy Content of Inner-Conductor Fiberglass Wrap	24%	24%	24%	24%	20%
Collar Material	High Manganese	Nitronic 40	Nitronic 40	Nitronic 40	Nitronic 40
Collar Shape	Round	Round	Round	Anti-Ovalized	Anti-Ovalized
Collar-Yoke Shim	None	None	None	None	76.2 mm**
Yoke Design				Revised	Revised
End Design	"yoke" set screws	"yoke" set screws	"yoke" set screws removed		

* Measured on conductor short samples

** 152.4 mm on diameter

INNER-LAYER STRESS

Change During Cool-Down

As we described in Reference 1, the coil is assembled into the collars with an azimuthal compressive stress. However, the thermal shrinkage coefficient of the coil in the azimuthal direction, integrated between room and liquid helium (LHe) temperatures, was measured to be 4.5×10^{-3} , compared to 3.0×10^{-3} for Nitronic-40 stainless steel, and 1.7×10^{-3} for Kawasaki stainless steel.⁶ During cool-down, the coil thus shrinks more than the collars, and the azimuthal compressive stress is expected to decrease.

The stress losses during the first cool-down of the five magnets described in this paper are summarized in Table II.a. They range from 25 to 30 MPa for magnets DD0027, DD0028, and DC0201. It is larger for magnet DD0026: 37 MPa. This larger loss is consistent with the fact that magnet DD0026 uses Kawasaki steel collars, whose integrated thermal shrinkage coefficient is lower than that of Nitronic-40 steel. The smallest loss is that of magnet DC0204: 21 MPa. Magnet DC0204 was also the magnet in this series with the lowest room-temperature pre-compression.¹ A possible explanation for this lower pre-compression is the lower epoxy content of the fiberglass wrap of the inner-layer conductor: 20% in weight for magnet DC0204, compared to 24% for the other magnets.

Table II. Summary of Mechanical Data of Selected BNL 4-cm-Aperture, 17-m-Long Collider Dipole Magnet Prototypes: a) Inner-Layer Stress Data, b) Outer Layer Stress Data, c) End-Force Data.

Magnet Name	Av. Inner Stress Change during 1st Cool-Down (MPa)	Av. Inner Stress after 1st Cool-Down (MPa)	Average Slope of Inner Stress vs. I^2 (MPa/kA ²)	Unloading Current (A)
DD0026	-37.3	15.6	0.52	6500
DD0027	-28.1	31.4	0.75	none
DD0028	-24.7	26.4	0.73	7000
DC0201	-29.8	25.4	1.05	6500
DC0204	-21.1	20.6	0.78	6500

Magnet Name	Av. Outer Stress Change during 1st Cool-Down (MPa)	Av. Outer Stress after 1st Cool-Down (MPa)	Average Slope of Outer Stress vs. I^2 (MPa/kA ²)	Unloading Current (kA)
DD0026	-16.3	31.7	0.18	none
DD0027	-16.2	39.2	0.27	none
DD0028	-24.6	17.0	0.22	none
DC0201	-10.2	25.5	0.24	none
DC0204	-18.3	26.5	0.22	none

Magnet Name	Total End-Force Change during 1st Cool-Down (kN)	Total End-Force after 1st Cool-Down (kN)	Total End-Force Slope vs. I^2 (kN/kA ²)
DD0026	-3.9	4.4	0.25
DD0027	-10.2	1.0	0.30
DD0028	-6.5	8.1	0.31
DC0201	18.8	25.6	0.37
DC0204	-2.7	10.6	0.29

As can be seen in Reference 1, the pre-compressions at LHe temperature of magnets DD0027, DD0028, and DC0201 are well correlated to the effective sizes of the inner layer package, while that of magnets DD0026 and DC0204 lie below the line. This is consistent with the particularities of these two magnets described above.

Change During Excitation

Figure 1 presents a typical example of the change in inner-layer stress as a function of current squared during an excitation of magnet DC0204. The four traces correspond to the pressures measured against the collar pole face of each quadrant. The arrows indicate the up- and down-ramps of the current.

It appears that at low currents the pressure exerted by the coil against the collar pole decreases linearly versus current squared. This is consistent with what can be expected from the Lorentz force, whose azimuthal component tends to compress the coil toward the midplane. As the current increases, however, the pressure flattens out and eventually reaches a constant level. The flattening of the pressure can in part be explained by the non-linear properties of the coil, whose Young's modulus is known to increase with increasing load.⁷

The fact that at high currents the stress does not change while the Lorentz force is still increasing indicates that the collar pole unloads, and that the average pressure exerted by the coil against the pole face becomes zero. (The non-zero values measured by the gauges must result from offsets introduced by differences between the active and compensating gauge reference resistance values.) In the following, we shall refer to as *unloading current*, the current at which the slope of the inner-layer stress versus I^2 becomes less than 10% of the initial slope.

The unloading of the coil inner layer illustrated in Figure 1 is typical of the magnets discussed in this paper. The unloading currents, summarized in Table II.a, were usually around 6500 A, except for magnet DD0027, which was excited up to 7200 A without its inner-layer stress reaching a plateau. Originally, this unloading was not intended to occur, and it had not been observed in magnets prior to DD0019.^{8,9} A prime reason why the actual magnets exhibit such behavior, while the earlier prototypes did not, is that their level of inner-layer pre-compression at LHe temperature is much lower: 20 MPa for magnet DC0204, compared to 55 MPa for magnet DD0017. Another reason is that for most of the recent magnets, the initial slope of the stress versus I^2 is larger: 0.78 MPa/kA² for magnet DC0204, compared to 0.56 MPa/kA² for magnet DD0017. The level of cold pre-compression is determined by the pre-compression at room temperature, which is itself controlled by the thickness of the brass shims inserted during assembly between the coil and the collar pole.¹ Magnets after, and including, DD0019 were deliberately assembled with a lower pre-compression to avoid overstressing the coil insulation during collaring. Thus obtaining a lower level of pre-compression in the cold state was not surprising. On the other hand, the slope of the stress versus I^2 was not expected to vary significantly.

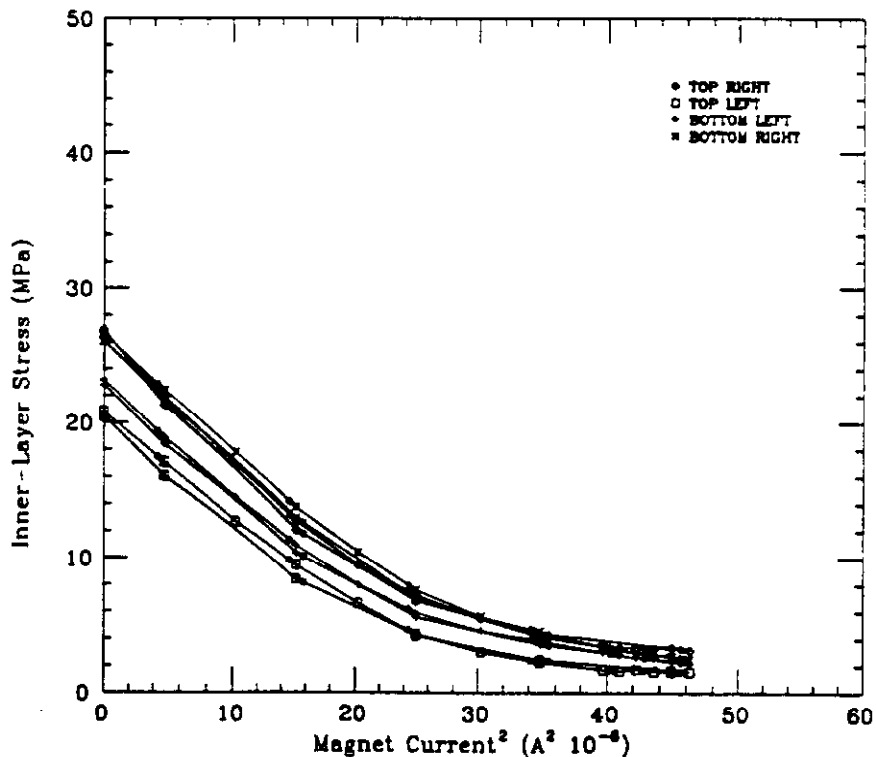


Figure 1. Change in the azimuthal pressure exerted by the coil inner layer against the collar pole during an excitation of BNL 4-cm-aperture, 17-m-long collider dipole magnet prototype DC0204 (the four traces correspond to the four quadrants of the coil)

Looking more closely at the data presented in Table II, it appears that there are large variations in the slopes even among the five magnets described in this paper. The smallest slope is observed for magnet DD0026, which uses round, Kawasaki steel collars: 0.52 MPa/kA². The largest is that of magnet DC0201, which uses anti-ovalized, Nitronic-40 collars: 1.05 MPa/kA². The other magnets—which use either round, Nitronic-40 collars, or anti-ovalized, Nitronic 40 collars, with shims at the tops and bottoms—occupy an intermediate position, with slopes between 0.7 and 0.8 MPa/kA². The dependence of the slope on the collar configuration suggests that it may be related to the collar-yoke interference at LHe temperature.

There is no practical way to directly measure the collar-yoke interference at LHe temperature, but it can be estimated. In Reference 1, we described how the horizontal and vertical diameters of the collared-coil assembly were regularly measured after completion of collaring. Let d_c designate the measured vertical diameter of the collared-coil assembly, and d_y the inner diameter of the yoke. Let us assume that the yoke midplane gap is entirely closed at the end of shell welding. For a magnet with no shims between the collar and the yoke, the vertical collar-yoke interference at room temperature, i_w , is given by

$$i_w = d_c - d_y. \quad (1a)$$

For a magnet with shims of thickness a between the collars and the yoke, interference is given by

$$i_w = d_c - d_y + 2a. \quad (1b)$$

The interference at LHe temperature, i_{LHe} , can then be estimated as

$$i_{LHe} = i_w - d_y(\alpha_c - \alpha_y) \quad (2)$$

where α_c is the integrated thermal shrinkage coefficient between room and LHe temperatures of the collar steel, and α_y is that of the yoke steel. The integrated coefficients used in the computation are: 3.0×10^{-3} for Nitronic-40, 1.7×10^{-3} for Kawasaki steel, and 2.0×10^{-3} for low carbon steel.

Figure 2 presents a summary plot of the initial slope of the inner-layer stress versus I^2 as a function of the estimated collar-yoke interference at LHe temperature. For each magnet, the slope is the average slope of the pressures measured against the collar pole face of each quadrant. (For magnets DD0027 and DD0028, which were equipped with two series of beam-type strain-gauge transducers, we selected the data from the transducers located at the minimum coil size location.) The collar-yoke interference is that calculated from Eq. (2) using the collar vertical deflection measured at the axial location of the beam-type strain-gauge transducers. The five magnets appear to lie on the same line. Thus, there appears to be a correlation between these two parameters.

There is not yet a clear understanding of why the slope of the inner-layer stress is so sensitive to the vertical collar-yoke interference. One plausible explanation follows: In the body of the magnet, the Lorentz force has two components—an azimuthal component, which tends to compress the coil towards the midplane, and a radial component, which tends to bend the collars outward, which is maximum at the midplane. If the yoke is tightly fitted to the collars, it provides an infinitely stiff support against the radial component of the Lorentz force. The collars do not bend, and the unloading of the collar pole results only from the compression of the coil under the azimuthal component of the Lorentz force. On the other hand, if the yoke is not tightly fitted to the collar, there can be a gap between the collar and the yoke, extending over a certain angle on both sides of the midplane. During energization, the collars bend and the coil deflects accordingly, with a maximum displacement at the midplane.

The arc length of the coil thus increases, resulting in a decrease of azimuthal compressive stress. In this case, the initial unloading of the collar pole results from two factors: 1) the coil compression under the azimuthal component of the Lorentz stress, and 2) the coil bending due to the radial component of the Lorentz force. This second factor accelerates the initial rate of unloading of the collar pole, resulting in a higher slope.

The amplitude of the bending moment that stretches the coil depends on the angular extent of the gap between the collars and the yoke with respect to the midplane. The larger the angle, the larger the bending moment. Rather than looking at the gap on both sides of the the midplane, one can also look at the perimeter of contact between the collar and the yoke on both sides of the pole plane. The smaller the perimeter, the larger the bending moment. If we assume that the yoke midplane gap is always closed, the perimeter of contact is completely determined by the amount of vertical interference between the collar and the yoke: the larger the interference, the larger the perimeter. This shows that the amplitude of the bending moment should be a decreasing function of the vertical collar-yoke interference. Because the azimuthal component of the Lorentz force is not expected to vary from magnet to magnet, the slope of the inner layer stress should follow the same dependence as the bending moment and be a decreasing function of the estimated vertical collar-yoke interference at LHe temperature, which is in qualitative agreement with what is observed in Figure 2. (On the other hand, as the current increases and the collars bend, the perimeter of contact between the collars and the yoke increases, resulting in a decreasing bending moment. The bending moment eventually becomes nil as the collars touch the yoke at the midplane. This decrease of the bending moment is another factor contributing to the flattening of the inner-layer stress observed in Figure 1 at high currents.)

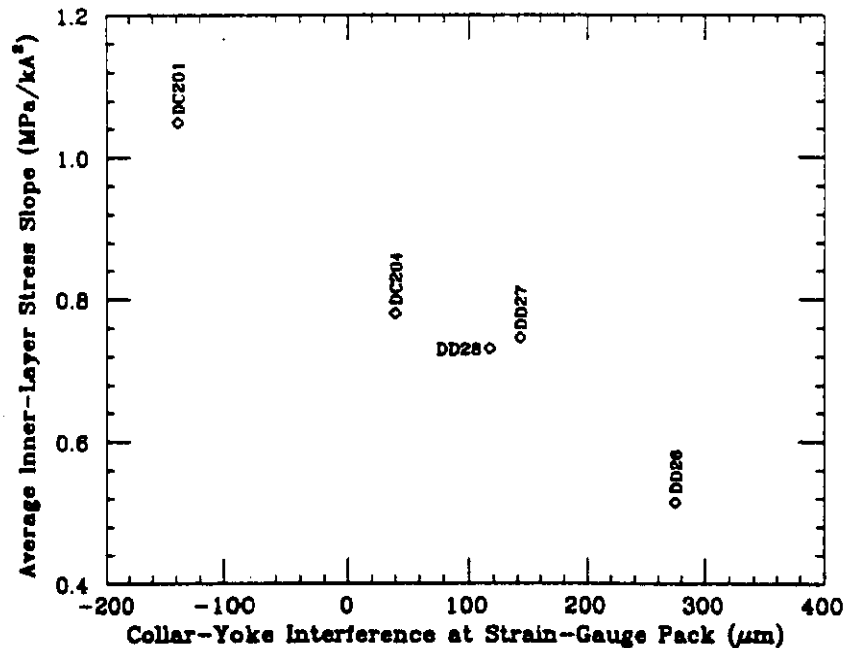


Figure 2. Correlation between the initial slope of the average inner-layer stress versus current squared and the estimated collar-yoke interference at LHe temperature of most recent BNL 4-cm-aperture, 17-m-long collider dipole magnet prototypes (the interference is that calculated at the axial location of the strain gauges).

If the above description is correct, the slope of the inner-layer stress provides an indirect measurement of the perimeter of contact between the collar and the yoke, and thus of the collar-yoke interference at LHe temperature. The fact that magnet DD0026 has the smallest slope conforms with our expectation that the use of Kawasaki steel should provide a tight fit between the collars and the yoke. The fact that magnet DC0201 has the largest slope confirms our fear that the 254 μm reduction of the collar vertical diameter might be excessive and that the collared-coil assembly might be loose inside the yoke at LHe temperature. The fact that magnet DC0204 has a slope similar to that of magnets DD0027 and DD0028 shows that the shims that were added on DC0204 acted mechanically as they were supposed to; that is, they increased the vertical collar-yoke interference in order to make a magnet originally designed as DC0201 behave like a round collar magnet.

We shall describe elsewhere² how the quench performance is affected by the bending of the collars and the unloading of the coil inner layer. One can, however, already mention that the coil unloading does not have the dramatic influence one might think it would have. As we said earlier, the Lorentz force can be resolved into two components: one radial and one azimuthal. The radial component is maximum at the midplane, but it exists on all the turns of the coil, including the pole turn. The pole turn is normally in contact with the face of the collar pole; the radial component of the Lorentz force thus introduces shear stress at the interface of the two. On the other hand, the azimuthal component of the Lorentz force compresses the coil toward the midplane. The pole turn thus tends to part from the face of the collar pole, and the frictional forces at the interface decrease. As the shear stress increases and the frictional forces decrease, the risk of conductor stick-slip motion, eventually leading to quenches, increases. All the magnets described in this paper exhibited training quenches that originated in the inner-layer pole turns, at currents of the order of or above the unloading currents. However, they all reached a plateau within a few percent of the estimated short-sample current limit, and all could be operated at low temperatures—thus higher force levels—without major problems. This shows that although the unloading cannot be ruled out as a cause of some of the training quenches, it is not a major threat to the magnet operation.

OUTER-LAYER STRESS

Change During Cool-Down

For the same reasons as those invoked for the inner-layer pre-compression, the outer-layer pre-compression is expected to decrease during cool-down. The cool-down data for the five magnets described in this paper are summarized in Table II.b. The changes during cool-down appear more erratic than for the inner layer, and they do not follow the same magnet-to-magnet pattern. Also, as can be seen in Reference 1, there is no clear correlation between the pre-compressions at LHe temperature and the effective sizes of the outer-layer package. The same lack of correlation was already observed at room-temperature; thus it is not surprising that it did not improve during cool-down. Two reasons can be found to explain this more erratic behavior and lack of correlation with the outer-layer size: 1) the mounting of the outer-layer transducers may be less reliable than that of the inner-layer transducers, and 2) the compression of the outer layer by the collars may be influenced by the inner layer.

Let us first discuss the reliability of the stress measurements. The stress data presented in Tables II.a and II.b are average values over the four coil quadrants. However, for most of the magnets, the standard deviation of the four outer-layer pressures is much larger than that of the inner-layer pressures. (The most dramatic case is magnet DD0027, with a standard deviation of 11.7 MPa for the outer-layer pressures after cool-down, compared to 2.3 MPa for the inner-layer pressures.) This difference can possibly arise from the mounting of the strain-gauge beams. In the case of the inner layer, the whole pole part of the collar laminations supporting the beams is cut in order to host a solid and accurately EDM'd stainless-steel base.⁵ In the case of the outer layer, the beams are also mounted

against a solid and accurately EDM'd backing plate, but the backing plate itself rests against a laminated surface. The roughness of this surface does not allow a perfect alignment of the beam, eventually leading to asymmetries between the four quadrants. Of course, this larger spread of the outer stress data raises questions about the reliability of the mean values given in Table II.b.

The question of the influence of the inner layer on the outer-layer pre-compression is more subtle. As the collars are mounted around the coil, they compress the two layers simultaneously. The two layers can therefore be considered as two parallel springs. The balance of forces in the collared-coil assembly then depends on the respective values of the two spring rates. If the inner-layer spring is stiffer, it dominates the outer-layer spring and determines the vertical deflection of the collars, and thus the azimuthal compressive stresses. On the other hand, both the inner layer and the collars apply a radial pressure on the outer layer. Because of Poisson's ratio, the arc length of the outer layer tends to increase, resulting in an increase of azimuthal stress. Both of these mechanisms result in variations of the outer-layer pre-compression which are not related to the outer-layer package size and which could account for the poor correlation that is observed. (Also, to be thorough, we would have to consider the frictional effects between the inner and outer layers, and between the coil and the collars. At this time, however, we do not have a clear picture of how these frictional effects influence the azimuthal pre-compressions.)

Change During Excitation

Figure 3 presents a typical example of the change in outer-layer stress as a function of current squared during an excitation of magnet DC0204. The four traces correspond to the pressures measured against the collar pole face of each quadrant. The arrows indicate the up- and down-ramps of the current. These data are from the same strain-gauge run as that of Figure 1. Despite the fact that they are widely spread, the four traces appear to be roughly parallel. This indicates that although one can have some doubt about the absolute values of the gauge readouts, their dynamic responses are consistent. They show that, in a manner similar to that of the inner layer, the outer layer has a tendency to unload from the pole, but the amplitude of this unloading is relatively small. The main reason for this smaller unloading is that the integral of the azimuthal component of the Lorentz force over the outer layer is much smaller than for the inner layer.

In the case of the inner layer, we saw that the initial slope of the stress versus I^2 was very sensitive to the vertical collar-yoke interference. One is curious to learn whether the outer layer exhibits the same correlation. Figure 4 presents a summary plot of the initial slope of the outer-layer stress versus I^2 as a function of the estimated collar-yoke interference at LHe temperature. For each magnet, the slope is the average slope of the pressures measured against the collar pole face of each quadrant. The collar-yoke interference is that calculated from Eq. (2) using the collar vertical deflection measured at the axial location of the beam-type strain-gauge transducers. For this plot, we deliberately chose the same X- and Y-scale range as for the plot in Figure 2. With this scaling, the slope of the outer-layer stress appears to be roughly constant. In the model developed above, this would indicate that the outer layer is much less sensitive to the bending moment resulting from the radial component of the Lorentz force, and that its rate of unloading is only determined by the azimuthal component of the Lorentz force, which does not change magnet to magnet. This lower sensitivity to the bending moment could possibly be explained by the fact that when the coil deflects to match the midplane bending of the collars caused by the radial component of the Lorentz force, the arc length of the outer layer does not increase as much as that of the inner layer, resulting in a smaller rate of loss of azimuthal compressive stress. One could also argue that as the current increases, the radial pressure exerted by the inner layer on the outer layer increases, resulting in an increase of the outer-layer arc length because of Poisson's ratio, partially compensating the loss of azimuthal compressive stress due to the other effects.

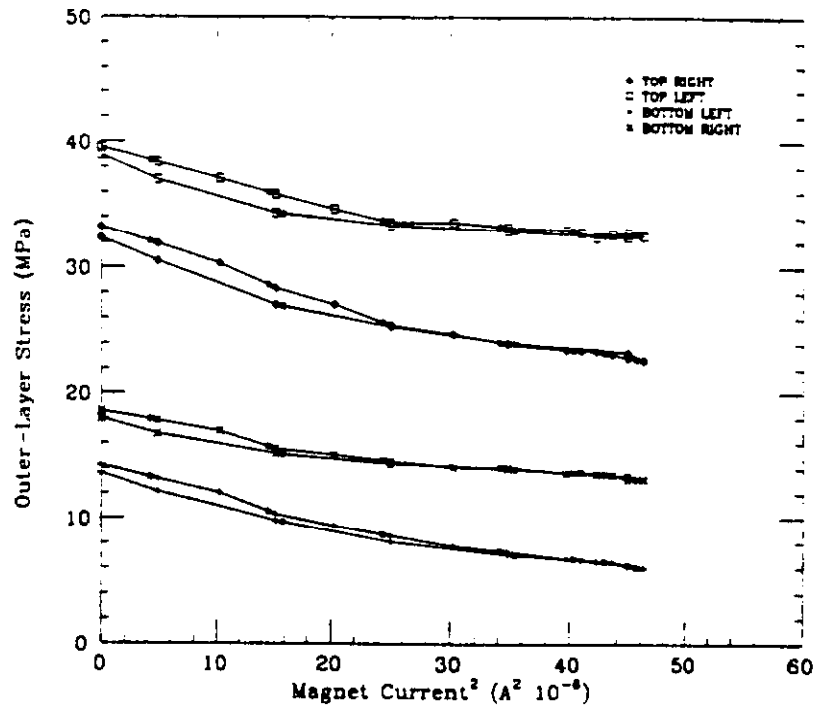


Figure 3. Change in the azimuthal pressure exerted by the coil outer layer against the collar pole during an excitation of BNL 4-cm-aperture, 17-m-long collider dipole magnet prototype DC0204 (the four traces correspond to the four quadrants of the coil).

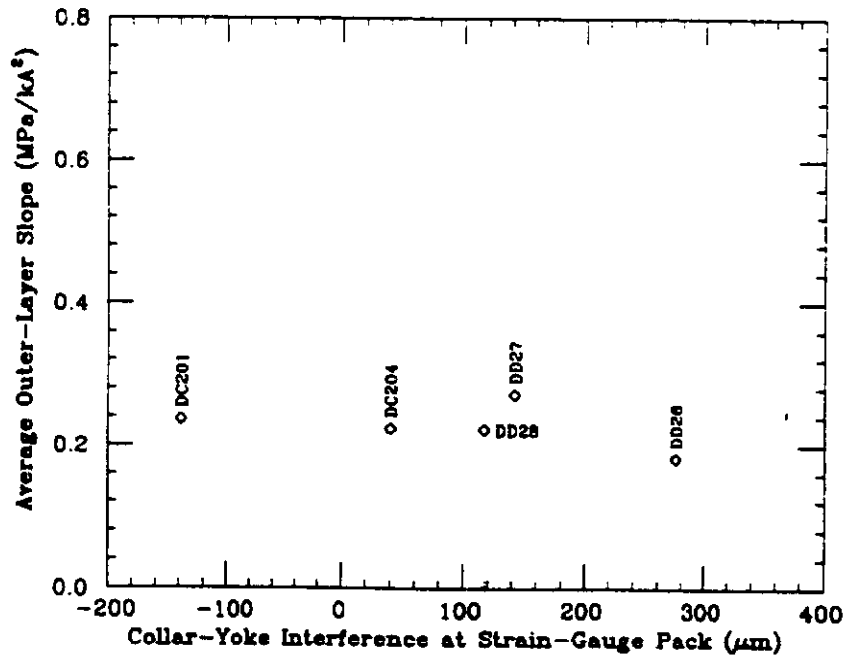


Figure 4. Correlation between the initial slope of the average outer-layer stress versus current squared and the estimated collar-yoke interference at LHe temperature of most recent BNL 4-cm-aperture, 17-m-long collider dipole magnet prototypes (the interference is that calculated at the axial location of the strain gauges).

END FORCE

Change During Cool-Down

Predicting the change in end-force during cool-down is not as straightforward as it is for the azimuthal compressive stress. As we described in Reference 1, the coil is loaded axially by means of screws that are set through the end-plate. The end-plate itself is anchored to a stainless-steel cylinder, called the *bonnet*, which is welded to the shell; during cool-down, the end-plate thus follows the shrinkage of the outer shell. If the presence of the yoke can be ignored, the change in end-force during cool-down is determined by the difference in thermal shrinkage coefficients in the axial direction between the coil and the outer shell. The integrated coefficient between room temperature and LHe temperature of the coil in the axial direction was measured at 2.5×10^{-3} , compared to 2.9×10^{-3} for the outer shell steel.⁶ From these data, the end-force is thus expected to increase during cool-down. On the other hand, the yoke laminations of the five magnets described in this paper were compactly stacked so that the yoke would behave mechanically as a monolith. As the outer shell is welded around the yoke, it is put into tension, and it applies a radial pressure on the yoke. This radial pressure results in a high friction at the interface between the yoke and the shell. During cool-down, the shell tries to shrink more than the monolithic yoke, whose integrated thermal shrinkage coefficient between room temperature and LHe temperature is only 2.0×10^{-3} . However, the high friction at the interface prevents the shell from doing so. The shell thus effectively stretches to match the thermal shrinkage of the yoke. In this situation, the change of end-force during cool-down is thus determined by the difference in thermal shrinkage coefficients in the axial direction between the coil and the yoke. From the aforementioned data, the end-force is thus expected to decrease during cool-down. In reality, the yoke is not purely monolithic, and part of the differential thermal shrinkage between the yoke and the shell is used to close gaps between the yoke laminations. The change in end-force during cool-down is thus expected to vary from magnet to magnet, depending on the amount of friction between the yoke and the shell, and on the compaction factor of the yoke.

The change in end-force during the first cool-down of the five magnets presented here is reported in Table II.c. For all but one magnet, the end-force decreased during cool-down. The magnet with increasing end-force was magnet DC0201, which used anti-ovalized, Nitronic 40 collars with no shims between the collar and the yoke. Magnet DC0201 was the magnet with the lowest vertical interference between the collar and the yoke. Also, it was the only magnet of the series whose yoke midplane gap was measured to be closed at the end of the yoke stacking, prior to the shell welding.¹ Therefore, the band clamps used to hold the two shell halves in place around the yoke in preparation for welding required less tension than on other magnets, resulting in a lower radial pressure on the yoke. (The band clamps are tightened until the gap between the two shell halves on each side of the magnet is 1.5 mm.) These two facts are consistent with low frictional forces at the interface between the yoke and the shell, which could eventually account for the increase in end-force during cool-down. For all other magnets, the yoke midplane gap was measured to be open at the end of the yoke stacking. To achieve the same gap between the shell halves, the band clamps therefore needed more tension, resulting in a higher radial pressure on the yoke, and thus higher frictional forces at the interface between the yoke and the shell. This is consistent with the observed decrease of end-force during cool-down. Also, one would expect the amplitude of this decrease to be somewhat related to the width of the yoke midplane gap: the larger the gap, the more radial pressure is needed to close it, and thus the higher the friction between the yoke and the shell. On the other hand, if the friction is higher, the shell is prevented from fully contracting to better match the shrinkage of the yoke, resulting in a larger decrease of end force. Among the magnets presented in Table II.c, DD0027 was the one with the largest yoke midplane gap; it also exhibited the largest decrease of end-force during cool-down.

As we have seen, the changes in end-force reported in Table II.c can be qualitatively explained. However, one can notice that the LHe-temperature values are more scattered than

what could be explained by these changes. This is because the room-temperature values were already scattered. As we described in Reference 1, the end-force is set during assembly to a nominal value of 4 kN. As the magnet is mounted on the test stand, bellows are welded at the periphery of the bonnet, connecting the magnet cold-mass to the He distribution. This welding induces a distortion of the bonnet, resulting in an increase of end-force that greatly varies from magnet to magnet. Aside from the fact that it is not reproducible, this increase is not thought to be a problem, since it goes in the direction of better axial loading. On the other hand, the fact that the end-force can decrease during cool-down and the fact that the sign and the amplitude of the change depend on a friction coefficient are more worrisome, for it is difficult if not impossible to predict the end-force level at LHe temperature and to ensure that this level will be sufficient. In the case of magnet DD0027, for instance, the end-force at LHe temperature ended up being very small, perhaps leading to poor quench performance. Studies are now underway to determine the quantitative relations that determine the change in end-force during cool-down and to devise a process to control them.

Change During Excitation

Figure 5 presents a typical example of end-force as a function of current squared during an energization of magnet DC0204. The four traces correspond to the four "bullet" gauge assemblies at the return end of the magnet (the return end is the magnet end opposite that where the current leads are connected). The arrows indicate the up- and down-ramps of the current. These data were taken during the same strain-gauge run as for Figures 1 and 3.

As expected, the end-force increases linearly as a function of current squared, indicating that the collared-coil assembly tends to expand inside the yoke. For the strain-gauge run presented in Figure 5, which was performed after magnet DC0204 had already been quenched several times, there is little variation in the slope of the end-force versus I^2 from zero to the maximum current. However, for most of the first strain-gauge runs after cool-down, the end-force exhibits a curvature at low currents, and the final slope is larger than the initial one. Typically, the DD series magnets exhibited a slope increase of the order of 40% during their first excitation to high current; the increase was about 20% for magnet DC0201, while there was no noticeable change for magnet DC0204. Such slope increase reveals that the coil end-parts stiffened during the first excitation, which can be interpreted as a sign that they were not properly loaded to begin with. In most cases, however, this problem goes away on subsequent excitations, and the amount of hysteresis between the up- and down-ramps is relatively small.

As we suggested, the collared-coil assembly tends to expand inside the yoke while energized. The rate of this expansion should be determined by the amount of friction between the collar and the yoke. As the friction increases, more of the end force can be shared by the yoke, decreasing the likelihood that the collared-coil assembly will expand. As for the inner-layer stress, we are therefore expecting to find a correlation between the slope of the end force versus I^2 and the estimated collar-yoke interference at LHe temperature. Figure 6 presents a summary plot of the slope as a function of the interference for the five magnets discussed in this paper. Because the slope changes as a function of current for some of the magnets, we selected the maximum-current slope, which we believe is more representative of the coil-end behavior. On the other hand, the estimated collar-yoke interference is that calculated from Eq. (2), using the average value of d_c over the magnet length.

Figure 6 shows a correlation similar to that of Figure 2, although the data are more scattered. Magnet DD0026 had the smallest end-force slope, 0.25 kN/kA². It was already the magnet with the smallest inner-layer stress slope, and it is consistent with our expectation of a tight collar-yoke fit, resulting from the use of Kawasaki steel collars. Magnet DC0201 had the highest slope, 0.37 kN/kA², which is consistent with our expectation of a loose collar-yoke fit, resulting from the use of anti-ovalized collars. The other magnets have slopes ranging from 0.29 to 0.31 kN/kA². As we already noticed on the inner-layer stress slope, the end-force slope shows that the shims that were added on the tops and bottoms of DC0204

collars acted mechanically as they were supposed to do; that is, they increased the amount of collar-yoke interference in order to make a magnet originally designed like DC0201 behave like DD0027 or DD0028. (DC0204 end-force slope, however, is slightly off the line defined by the other magnets, revealing that the collar-yoke interference at LHe temperature may be larger than estimated. This error could come from the fact that in calculating the thickness of the shims to be used in Eq. (1b), we neglected the double adhesive tape that secures them on the tops and bottoms of the collars.)

The most interesting conclusion from Figures 2 and 6 is that the inner-layer stress slope and the end-force slope exhibit a similar dependence on the estimated vertical collar-yoke interference at LHe temperature. This sensitivity of magnet mechanical behavior to collar-yoke interference raises a number of concerns, the most serious of which is that collars and yoke are both laminated. Their contact surface is thus very rough, creating a risk of stick-slip motions of the collars inside the yoke during cool-down and subsequently during excitation. These sudden motions of collars during excitation can eventually lead to quenches in the outer layer of the coil. (Unlike the yoke, the collars are not monolithic, and gaps subsist between the collar packs where bending can occur.) This is certainly a clue for the predominance of outer-layer quenches that were observed during the quench-testing of these magnets.²

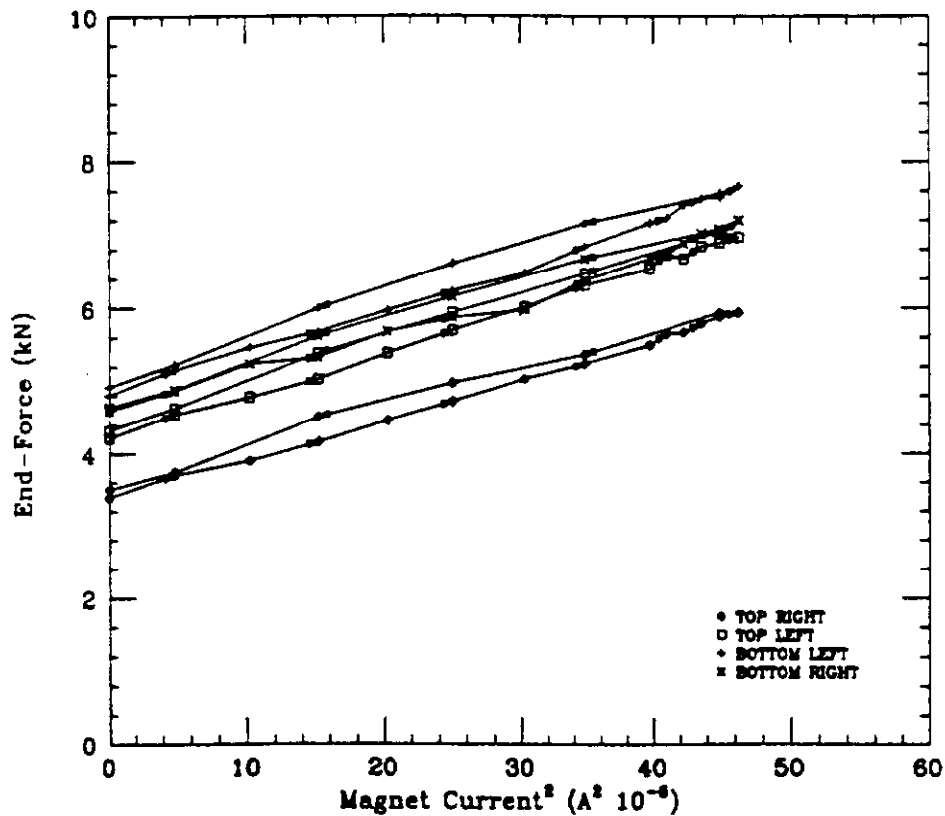


Figure 5. Change in the axial force exerted by the coil against the end-plate loading screws during an excitation of BNL 4-cm-aperture, 17-m-long collider dipole magnet prototype DC0204 (the four traces correspond to the four loading screws).

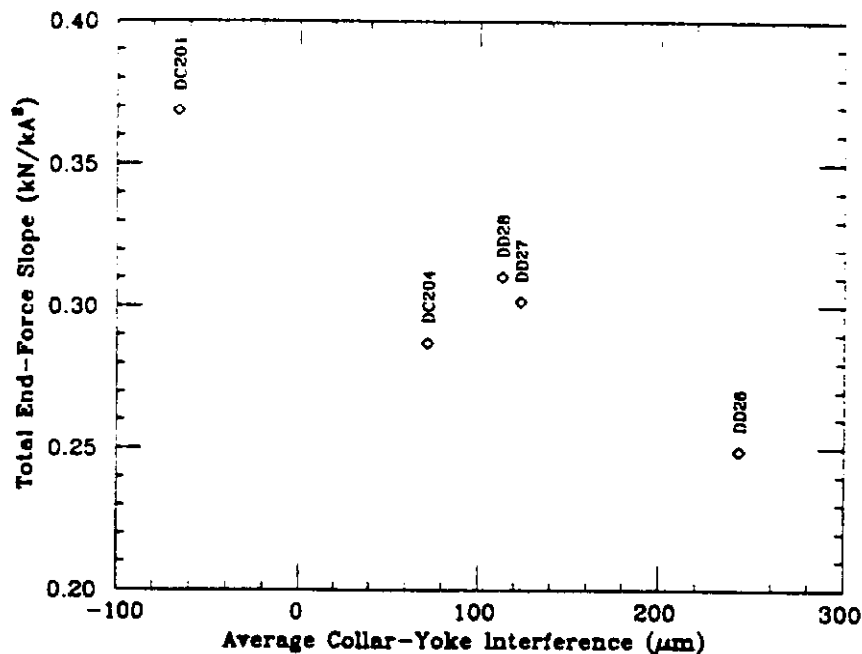


Figure 6. Correlation between the final slope of the total end-force versus current squared and the estimated collar-yoke interference at LHe temperature of most recent BNL 4-cm-aperture, 17-m-long collider dipole magnet prototypes (the interference is that calculated in average over the magnet length).

CONCLUSION

In this paper, we reviewed the mechanical data during cool-down and excitation of the five most recent BNL 4-cm-aperture, 17-m-long SSC dipole magnet prototypes. We successively analyzed the changes in azimuthal compressive stress in the coil inner and outer layers, and the changes in axial compressive load at the coil ends. We saw that for most of the magnets, the azimuthal pressure exerted by the coil inner layer against the collar pole decreased to zero during energization, revealing a possible unloading of the pole. We found that the rate of decrease of the inner-layer stress and the rate of increase of the end-force during energization were correlated to the estimated vertical interference between the collars and the yoke at LHe temperature. These correlations are similar in trend: the tighter the clamping of the collared-coil assembly by the yoke, the smaller the rate of change. We also saw that for most of the magnets, the end-force decreased during cool-down, and the amplitude of this decrease was somewhat erratic, varying greatly from magnet to magnet. The next step is to analyze how these variations in mechanical behavior influence the quench performance and eventually to determine which are preferable for the magnet operation. This discussion will be the subject of a future paper.²

REFERENCES

1. A. Devred, T. Bush, et al., "Status of 4-cm-Aperture, 17-m-Long SSC Dipole Magnet R&D Program at BNL. Part I: Magnet Assembly," to appear in the proceedings of the 3rd Annual International Industrial Symposium on the Super Collider, Atlanta, GA, USA, March 13-15, 1991.
2. A. Devred, T. Bush, et al., "Status of 4-cm-Aperture, 17-m-Long SSC Dipole Magnet R&D Program at BNL. Part III: Quench Performance," to be published.
3. T. J. Peterson and P. O. Mazur, "A Cryogenic Test Stand for Full Length SSC Magnets with Superfluid Capability," *Supercollider 1*, M. McAshan, ed., 1989, pp. 551-559.
4. J. Strait, M. Bleadon, et al., "Fermilab R&D Test Facility for SSC Magnets," *Supercollider 1*, M. McAshan, ed., 1989, pp. 561-572.
5. C. L. Goodzeit, M. D. Anerella, et al., "Measurement of Internal Forces in Superconducting Accelerator Magnets with Strain Gauge Transducers," *IEEE Trans. Magn.*, **25**, No. 2, 1989, pp. 1463-1468.
6. C. L. Goodzeit, private communication.
7. T. Ogitsu, K. Machata, et al., "Mechanical Hysteresis of Superconducting Coils," to be published.
8. J. Tompkins, M. Chapman, et al., "Performance of full-length SSC model dipoles: results from 1988 tests," *Supercollider 1*, M. McAshan, ed., 1989, pp. 33-49.
9. C. Goodzeit, P. Wanderer, et al., "Status Report on SSC Dipole R&D," to appear in the Proceedings of the 10th Workshop on the INFN Eloisatron Project—New Techniques for Future Accelerators, High Energy Intensity Storage Rings, Status and Prospects for Superconducting Magnets, Erice, Italy, October 16-24, 1989.